



Research paper

Solubility of CePO₄ monazite and YPO₄ xenotime in H₂O and H₂O–NaCl at 800 °C and 1 GPa: Implications for REE and Y transport during high-grade metamorphismPeter Tropper^{a,b,*}, Craig E. Manning^b, Daniel E. Harlov^c^a Institute of Mineralogy and Petrography, Faculty of Geo- and Atmospheric Sciences, University of Innsbruck, Innrain 52, A-6020 Innsbruck, Austria^b Department of Earth and Space Sciences, University of California, Los Angeles, CA 90095-1567, USA^c Helmholtz Zentrum Potsdam, Deutsches GeoForschungsZentrum, Telegrafenberg, D-14473 Potsdam, Germany

ARTICLE INFO

Article history:

Received 6 July 2010

Received in revised form 11 January 2011

Accepted 12 January 2011

Available online 19 January 2011

Editor: D.B. Dingwell

Keywords:

Monazite

Xenotime

Solubility

Piston cylinder experiments

Brines

REE mobility

ABSTRACT

Monazite and xenotime are important accessory minerals in metasediments because they host REE and are useful for geochronology and geothermometry. It is therefore essential to understand their behavior during metasomatic processes that attend metamorphism and subduction. In order to constrain the solubility of monazite and YPO₄ xenotime at high pressure and temperature, we carried out weight-loss experiments on synthetic single crystals of CePO₄ (monazite) and YPO₄ (xenotime) using hydrothermal piston-cylinder methods at 800 °C and 1 GPa, in H₂O and H₂O–NaCl fluids. Results indicate that CePO₄ and YPO₄ dissolved congruently, and that their solubilities in pure H₂O are very low: 0.04 ± 0.04 and 0.25 millimolal, respectively. The solubility of CePO₄ rises to an increasing extent with added NaCl, to 7.94 ± 0.07 millimolal at 50 mol% NaCl. In contrast, the solubility of YPO₄ rises to a decreasing degree with increasing NaCl, to 4.36 ± 0.08 millimolal at 50 mol% NaCl. Best fit equations for the solubilities of the two phases are

$$m_{\text{CePO}_4} = 3.56 \cdot 10^{-5} + 5.82 \cdot 10^{-3} X_{\text{NaCl}} + 1.97 \cdot 10^{-2} X_{\text{NaCl}}^2$$

and

$$m_{\text{YPO}_4} = 2.48 \cdot 10^{-4} + 1.26 \cdot 10^{-2} X_{\text{NaCl}} - 8.89 \cdot 10^{-3} X_{\text{NaCl}}^2$$

The solubility of YPO₄ is greater than that of CePO₄ at NaCl mole fractions (X_{NaCl}) of 0.00–0.27. The solubility enhancement behavior implies that Ce dissolves as anhydrous chloride complexes, whereas Y forms mixed Cl–OH solutes. The results provide a simple mechanism for redistributing REE and Y in deep-crustal and upper mantle environments. The H₂O/Ce ratio inferred for subduction-zone melts and silicate-rich fluids can also be produced by a CePO₄-saturated fluid with $X_{\text{NaCl}} = 0.1$. In addition, neutral-pH H₂O–NaCl fluids can transport substantial REE and Y, obviating the need to invoke highly acid solutions in environments where they are unlikely.

© 2011 Elsevier B.V. All rights reserved.

1. Introduction

Monazite and xenotime are important accessory phases in metamorphic and igneous rocks (e.g., Spear and Pyle, 2002). Occurring in a range of metamorphic lithologies and settings, these phosphates have great utility as prograde index minerals that can be used for geochronology (e.g. Harrison et al., 2002; Wing et al., 2003; Kohn and Malloy, 2004; Corrie and Kohn, 2008; Janots et al., 2008, 2009). They represent important reservoirs for rare-earth elements

(REE), and the exchange of REE between orthophosphates and silicates such as garnet provides information about metamorphic history (Gratz and Heinrich, 1997; Andrehs and Heinrich, 1998; Pyle and Spear, 1999, 2000; Pyle et al., 2001). REE orthophosphates also play an important role in controlling REE, U and Th distribution during granitoid crystallization (Overstreet, 1967; Miller and Mittlefehldt, 1982; Montel, 1986, 1993; Rapp and Watson, 1986; Cuney and Friedrich, 1987). Their high durability and resistance to metamictization make the REE phosphates potential hosts for nuclear waste disposal (e.g., Boatner and Sales, 1988; Ewing, 2001; Read and Williams, 2001; Boatner, 2002; Ewing and Wang, 2002).

Experimental studies of monazite and xenotime solubility in H₂O show that solubilities rise with pressure and temperature, but are generally very low over a wide range of igneous and metamorphic

* Corresponding author at: Institute of Mineralogy and Petrography, Faculty of Geo- and Atmospheric Sciences, University of Innsbruck, Innrain 52, A-6020 Innsbruck, Austria.

E-mail address: peter.tropper@uibk.ac.at (P. Tropper).

conditions unless pH is acidic or temperatures are extremely high (e.g., Wood, 1990a,b; Wood and Williams-Jones, 1994; Haas et al., 1995; Devidal et al., 1998; Poitrasson et al., 2004; Cetiner et al., 2005; Schmidt et al., 2007; Pourtier et al., 2010).

The low monazite and xenotime solubilities returned by experimental studies make it difficult to explain their natural associations with metasomatic features in igneous and metamorphic rocks, such as hydrothermal alteration assemblages, veins and skarns (Cesbron, 1989; Philippot and Selverstone, 1991; Bingen et al., 1996; Gieré, 1996; Poitrasson et al., 1996, 2000; Townsend et al., 2000; Seydoux-Guillaume et al., 2002; Roland et al., 2003; Hetherington and Harlov, 2008; Bosse et al., 2009). Either fluid flux must be generally high enough to mobilize relatively insoluble essential constituents, or the pH must in every case be acidic. An alternative mechanism for the dissolution and transportation of orthophosphate components is a high alkali halide concentration in the fluid phase. It has been proposed that REE (and by extension, Y) mobility may be enhanced by dissolved halogens (Pan and Fleet, 2002; Schmidt et al., 2007; Antignano and Manning, 2008a; Pourtier et al., 2010). In a wide range of crustal and mantle fluids, the halogens are present in solution as dissolved alkali-halides — in some cases as highly concentrated brines (e.g., Touret, 1985, 2001; Markl and Bucher, 1998; Markl et al., 1998). For example, alkali-halide brines play an important role in mass transport and mineral-fluid-melt phase equilibria in the lower crust (e.g., Newton et al., 1998; Yardley and Graham, 2002; Newton and Manning, 2010; Rapp et al., 2010). In addition, subduction-zone fluids from some environments may also contain significant concentrations of dissolved salts (e.g., Philippot and Selverstone, 1991; Selverstone et al., 1992; Nadeau et al., 1993; Scambelluri et al., 1998; Scambelluri and Philippot, 2001). High NaCl concentrations have also been proposed as a mechanism for explaining trace element abundances in arc magmas (Keppler, 1996).

In this study, we investigated the hypothesis that dissolved NaCl influences monazite and xenotime solubilities. We report new measurements of CePO_4 monazite and YPO_4 xenotime solubility in H_2O and H_2O –NaCl at 800 °C and 1.0 GPa, in order to put experimental constraints on the dependence of REE and Y solubility on X_{NaCl} at fixed P – T conditions. The data indicate that CePO_4 and YPO_4 have a very low solubility in H_2O , that NaCl enhances solubilities, and that different dependences of monazite and xenotime solubility on the NaCl content implies contrasting complexing behavior for Ce and Y in fluids. In the presence of NaCl, geologic fluids will have a high capacity to dissolve and transport LREE and to a certain extent HREE at high P and T .

2. Experimental methods

Most experiments used synthetic crystals of CePO_4 monazite and YPO_4 xenotime. Crystals of CePO_4 (monazite) and YPO_4 (xenotime) were grown from a very fine CePO_4 or YPO_4 precipitate thoroughly mixed dry with a Pb-free flux ($\text{Na}_2\text{CO}_3:\text{MoO}_3 = 1:3$). The CePO_4 or YPO_4 were synthesized by mixing stoichiometric amounts of REE (NO_3) $\cdot 6\text{H}_2\text{O}$ and $(\text{NH}_4)_2\text{HPO}_4$ in solution. The resulting precipitate was allowed to settle and the excess fluid poured off. The precipitate was then dried and ground up. Twenty grams of flux mixed with 0.8 g precipitate was packed in a loosely covered Pt crucible and taken up to a temperature of 1280 °C at 1 atm. The molten flux was 'soaked' at 1280 °C for 15 h, which was then cooled down to 870 °C with a cooling rate of 3 °C per hour (Cherniak et al., 2004). This resulted in the nucleation and growth of 0.1 to 5 mm size euhedral CePO_4 or YPO_4 crystals at the bottom of the Pt crucible.

Small crystals (0.35–3.7 mg) optically free of flux–melt inclusions were selected for the experiments. One run used natural monazite from a beach sand in Cleveland Co., North Carolina (Ward's collection #192). Its chemical composition is given in Table 1. In each experiment a single crystal was placed in an inner Pt envelope or a 1.6 mm OD Pt capsule. To facilitate H_2O penetration while ensuring crystal containment during experiments, the encapsulating material was lightly crimped and

Table 1
Average composition of natural monazite (wt.%).

P ₂ O ₅	28.42	0.186
SiO ₂	1.17	0.086
ThO ₂	7.99	0.554
UO ₂	0.27	0.086
Y ₂ O ₃	0.55	0.200
Ce ₂ O ₃	29.41	0.237
La ₂ O ₃	13.44	0.217
Pt ₂ O ₃	3.08	0.036
Nd ₂ O ₃	11.15	0.260
Sm ₂ O ₃	1.87	0.100
Gd ₂ O ₃	1.01	0.136
Tb ₂ O ₃	0.07	0.081
Dy ₂ O ₃	0.08	0.058
Ho ₂ O ₃	0.02	0.039
Er ₂ O ₃	0.02	0.031
Yb ₂ O ₃	0.02	0.028
CaO	0.90	0.071
PbO	0.12	0.012
F	0.60	0.021
Total (—O≡F)	99.94	

Explanation: Mean of 5 monazite analyses determined by wavelength-dispersive electron microprobe analysis using a Cameca SX50 at the University of Massachusetts, Amherst. Operating conditions included a focused 1 μm beam diameter, 15 kV accelerating voltage, and 15 nA beam-current. Standards were cheralite (Th), UO₂ (U), synthetic phosphates (Y + REE), plagioclase (Si), fayalite (Fe), pyrite (S), fluorapatite (Ca and P), synthetic fluorides (Sr and F), chlorides (Cl), and GaAs (As). Data reduction employed the Cameca PAP correction procedure. Al₂O₃, Lu₂O₃ and FeO, S, As and Cl were below detection limit.

perforated two to four times with a needle. The inner capsule precisely weighed quantities of NaCl and H₂O were then placed in an outer 3.5 mm OD Pt capsule with a 0.20 mm wall thickness (Table 1). The capsule was then sealed by arc welding. The double capsule assembly was held at 115 °C for ≥ 3 h to check for leakage.

All experiments were conducted in an end-loaded, piston-cylinder apparatus using 25.4 mm diameter graphite–NaCl furnace assemblies (Bohlen, 1984; Manning and Boettcher, 1994). Each capsule was placed horizontally in the furnace, packed in NaCl, and covered with a piece of Pt foil to prevent puncture by the thermocouple. Temperature was monitored and controlled using Pt/Pt₉₀Rh₁₀ thermocouples (± 3 °C estimated precision). Pressure was monitored using a Heise gauge (± 0.01 GPa estimated precision).

At the end of each experiment, power to the apparatus was cut, causing quench to <100 °C in ≤ 30 s. After quenching, the outer capsule was pierced with a needle, dried for 15 min at 115 °C, and then 15 min at 400 °C. The capsule assembly was then opened and inspected, and the crystals extracted, cleaned and weighed. Comparison of H₂O weight before and after experiments showed that there was no significant change during runs (+0.5 to −0.3%; Table 2). Solubilities were calculated using H₂O added to an experiment ("H₂O in", Table 2). The intrinsic oxygen fugacity of the experimental apparatus at these conditions is near the Ni–NiO buffer (Newton and Manning, 2005), so Ce can be assumed to be trivalent. All run products were examined optically with a binocular microscope; selected run products were examined with a scanning electron microscope.

Reported weights represent the average of three replicate weighings, with uncertainties determined by repeated weighings of a standard. We used a Mettler UMX2 ultra-microbalance (1σ = 0.2 μg) to determine crystal weights; all other weighings were done on a Mettler M3 microbalance (1σ = 2 μg). Uncertainties in CePO_4 and YPO_4 concentrations are reported as 1σ and reflect propagated weighing errors only.

3. Results

Results are given in Table 1. Run products included partly dissolved starting crystals (Figs. 1 and 2) and fine-grained, white or colorless quench

Table 2
Experimental results at 800 °C, 1 GPa.

Run	Time (h)	H ₂ O in (mg)	H ₂ O out (mg)	NaCl in (mg)	X _{NaCl}	Crystals in (mg)	Crystals out (mg)	Molality
<i>CePO₄-H₂O-NaCl</i>								
Mnz-18	90	35.893	35.935	0	0	1.1635	1.1632	0.00004(3)
Mnz-2	12	34.192	34.258	11.290	0.092	2.4377	2.4308	0.00086(4)
Mnz-20	90	30.980	–	11.168	0.100	0.3236	0.3168	0.00093(4)
Mnz-5	12	26.027	26.123	20.866	0.198	1.8713	1.8596	0.00192(5)
Mnz-15	12	25.323	25.303	35.205	0.300	1.2125	1.1927	0.00333(5)
Mnz-19	92	22.854	22.962	49.350	0.399	0.3676	0.3380	0.00551(5)
Mnz-22	90	17.627	17.589	56.710	0.498	0.4289	0.3960	0.00794(7)
<i>Natural monazite-H₂O-NaCl</i>								
Mnz-14 ^a	12	25.032	25.110	34.914	0.301	48.738 ^b	48.710 ^b	0.0048(5)
<i>YPO₄-H₂O-NaCl</i>								
Xnt-4	12	41.618	41.757	0	0	2.3541	2.3522	0.00025(4)
Xnt-2	12	33.159	33.277	11.467	0.096	2.7266	2.7189	0.00127(5)
Xnt-7	12	25.901	26.032	20.910	0.199	1.8713	1.8596	0.00247(6)
Xnt-5	12	21.159	21.272	27.558	0.286	3.2445	3.2316	0.00332(7)
Xnt-9	12	19.961	19.993	42.984	0.399	1.0722	1.0588	0.00366(8)
Xnt-13	12	20.373	20.373	65.005	0.496	2.0612	2.0449	0.00436(8)

Parentetical entries reflect propagated weighing errors (1 σ). The 1 σ error in X_{NaCl} is 1.7 $\times 10^{-5}$.

^a From monazite sand, Cleveland County, NC, USA; UCLA mineral collection #MS 1762.

^b Solubility determined from inner capsule weight change because crystal broke during experiment.

solids. Only minor quench was observed in the H₂O–NaCl experiments (Figs. 1D, 2C). The original grains displayed rounded edges and, in some cases, significant new subhedral octahedral overgrowths (Fig. 1B). The

absence of any residual crystals on grain surfaces indicates that CePO₄ and YPO₄ dissolve congruently in H₂O–NaCl.

Run duration necessary to attain equilibrium was determined in two experiments at 800 °C, 1 GPa and X_{NaCl} = 0.1 (Table 1). Experiments of 12 h (Mnz-2) and 90 h (Mnz-20) gave the same solubility of respectively 0.00086 and 0.00093 m, within 1 σ propagated weighing uncertainty of 4 $\times 10^{-5}$ m. Attainment of constant solubility within 12 h is consistent with equilibration rates in other solubility measurements at high T and P (e.g., Caciagli and Manning, 2003; Tropper and Manning, 2005). In addition, Schmidt et al. (2007) carried out in-situ dissolution experiments in a diamond anvil cell in the system monazite–H₂O–HCl \pm NaCl and found that equilibrium between fluid and crystal was attained in 50 min at temperatures of ≥ 300 °C.

Starting synthetic xenotime and monazite crystals were carefully screened to avoid grains with visible flux–melt inclusions. However, in several cases, examination of partially dissolved monazite crystals after runs revealed pits on the surface (Fig. 1C). These pits are interpreted to be sites of undetected flux–melt inclusions, from which the inclusion material was dissolved into the fluid. Preferential dissolution of flux–melt inclusions where they intersect the dissolving crystal surface yields a higher apparent solubility. The effect is expected to be greatest at low X_{NaCl} where monazite solubility is lowest. One experiment in pure H₂O revealed possible etch pits during post-mortem examination, and was discarded. However, at high X_{NaCl} (Fig. 1C), the much greater solubility means that any dissolution of a minute mass of inclusion material does not contribute significantly to the measured solubility. This interpretation is supported by the fact that experiment Mnz-19, with trace inclusions (Fig. 1C), returned a solubility consistent with the trend defined by experiments at higher and lower NaCl content (Fig. 3), in which no evidence for flux–melt inclusions was noted.

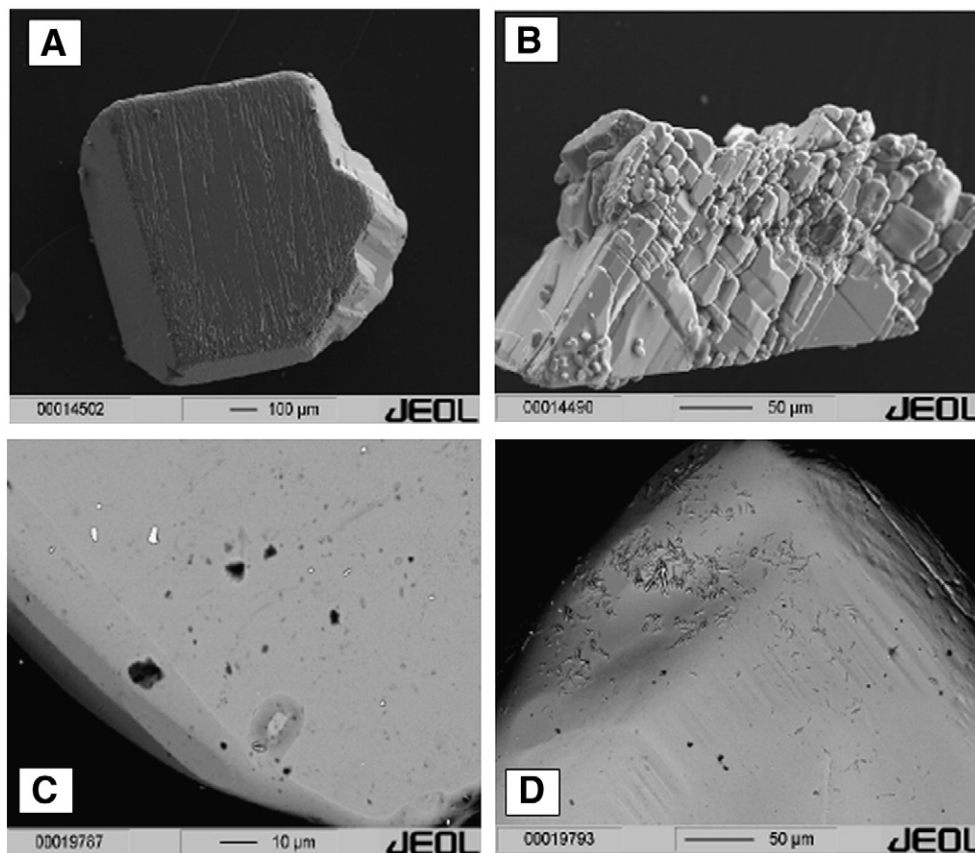


Fig. 1. Backscatter electron (BSE) images of the CePO₄ reaction products after the solubility experiments. (A) CePO₄ crystal after dissolution at X_{NaCl} = 0.2 (Mnz-5). (B) Fragment of CePO₄ crystal dissolved in X_{NaCl} = 0.3 fluid (Mnz-15), displaying dissolution grooves and recrystallization. (C) Close-up of the CePO₄ product crystal after dissolution in X_{NaCl} = 0.4 fluid, showing dissolution pits interpreted to represent preferential dissolution of flux–melt inclusions (Mnz-19). (D) CePO₄ crystal after dissolution in X_{NaCl} = 0.5 fluid, with a minute quench crystals adhering to the surface (Mnz-22).

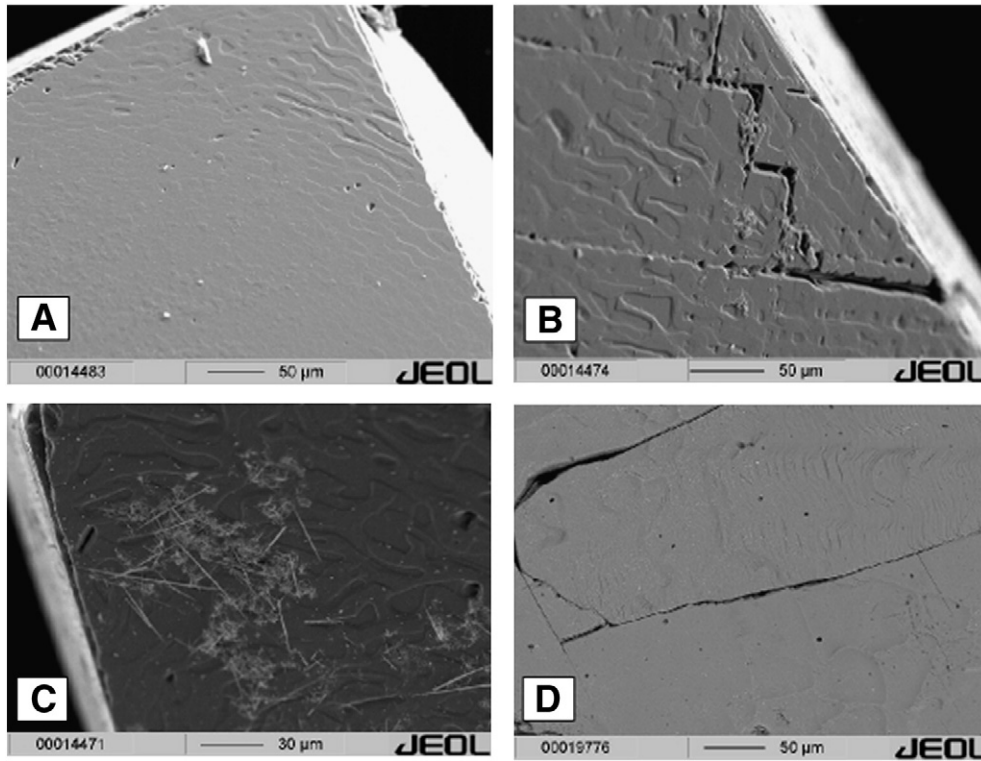


Fig. 2. Backscatter electron (BSE) images of the YPO₄ reaction products after the solubility experiments. (A) YPO₄ crystal after dissolution in X_{NaCl} = 0.2 fluid (Xnt-7), showing subtle dissolution grooves. (B, C) YPO₄ crystal from experiment Xnt-5, at X_{NaCl} = 0.3, displaying strong dissolution-patterning on crystal faces (B) and fine quench crystals (C). (D) YPO₄ crystal after dissolution in X_{NaCl} = 0.5 fluid, showing dissolution grooves (Xnt-13).

The experimental results at 800 °C and 1 GPa indicate very low CePO₄ and YPO₄ solubilities in H₂O of 0.04 ± 0.03 millimol/kg H₂O and 0.25 ± 0.04 millimol/kg H₂O (Table 1). The solubility of CePO₄ in H₂O is <3σ of the weighing error and thus below the nominal detection limit of 0.09 millimolal.

The solubility of CePO₄ in H₂O–NaCl fluids at 800 °C, 1 GPa, increases with increasing NaCl, to 7.94 ± 0.07 millimol/kg H₂O at X_{NaCl} = 0.498 (Fig. 3). This corresponds to an increase of ~200 times over the investigated range. Weighted least-squares regression of the data to a second-order polynomial gives:

$$m_{\text{CePO}_4} = 3.56 \cdot 10^{-5} + 5.82 \cdot 10^{-3} X_{\text{NaCl}} + 1.97 \cdot 10^{-2} X_{\text{NaCl}}^2 \quad (1)$$

where m_{CePO_4} is CePO₄ molality ($R^2 = 0.998$). The fit was forced through the measured pure-H₂O value to facilitate assessment of the solubility enhancement (see below). Given that this point is below the nominal detection limit of 0.09 millimolal, an alternative approach is to set this datum at the midpoint between 0.00 and 0.09 millimolal, with equal probability of any solubility between these limits. The best fit under this scenario returns a constant of 9.85×10^{-5} millimolal with R^2 remaining at 0.998.

In contrast to CePO₄, the solubility of YPO₄ in H₂O–NaCl at 800 °C, 1 GPa, initially increases steeply with increasing NaCl, indicating that YPO₄ solubility is greater than that of CePO₄ in H₂O-rich fluids. However, the rise in YPO₄ solubility with salinity decreases with increasing X_{NaCl}. The different dependence on NaCl concentration causes CePO₄ and YPO₄ to be roughly two times more soluble at X_{NaCl} ~ 0.5, the highest salinity investigated (Table 2; Fig. 3). Weighted least-squares regression of the data to a second-order polynomial gives:

$$m_{\text{YPO}_4} = 2.48 \cdot 10^{-4} + 1.26 \cdot 10^{-2} X_{\text{NaCl}} - 8.89 \cdot 10^{-3} X_{\text{NaCl}}^2 \quad (2)$$

where the fit is again forced through the pure H₂O datum ($R^2 = 0.992$).

The solubility of a natural monazite at X_{NaCl} = 0.3 was found to be 4.8 ± 0.5 millimolal. This is higher than the solubility of CePO₄ (3.33 ± 0.05 millimolal) at the same X_{NaCl}. The difference is most likely due to the presence of additional, soluble components (e.g., Nd, La, Th, U, Si, and Ca) in the natural monazite.

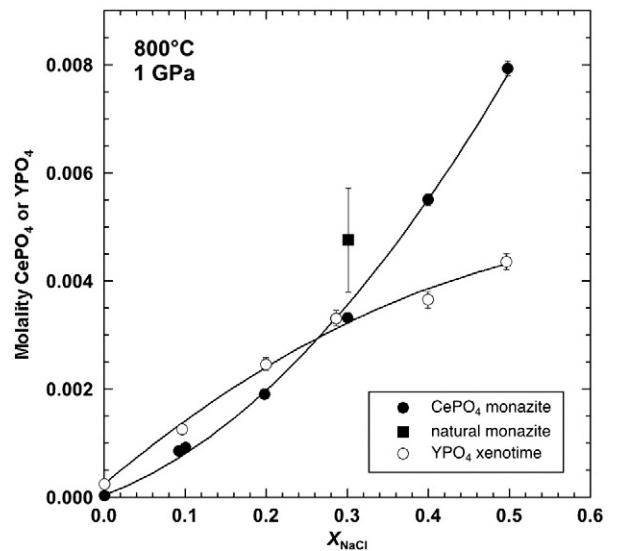


Fig. 3. Orthophosphate molality versus X_{NaCl} at 800 °C and 1 GPa. Molal solubility of natural monazite was calculated assuming congruent dissolution. The error bars are 2σ and are calculated based on the weighing uncertainties. The solid lines are the fitted solubilities from Eqs. (1) and (2).

4. Discussion

4.1. Solubility in H₂O

We find that YPO₄ is at least 1.5 times more soluble than CePO₄ in pure H₂O at 800 °C and 1 GPa. This result is in nominal conflict with the general observation that monazite is more common than xenotime in hydrothermal veins and other metasomatic features, which implies greater solubility of LREE relative to HREE and Y (e.g., Schmidt et al., 2007). However, REE and Y dissolution in natural fluids are controlled by ligands other than H₂O or phosphate, such as chloride, fluoride, sulfate, and aluminosilicates, all of which can be expected to occur in varying proportions. Consequently, experimental results obtained using pure H₂O do not necessarily give useful insights into the behavior of these minerals in metasomatic contexts.

Comparison of previous high *P*–*T* experimental monazite solubility data with the results from this investigation reveals substantial differences (Fig. 4). Results from solutions with near-neutral pH and up to 4 molal NaCl ($X_{\text{NaCl}}=0.07$) are included in the comparison. Despite substantial scatter, the combined 0.2 GPa data set of Gibert and Montel (1996) and Pourtier et al. (2010) on NdPO₄ give the highest solubility in H₂O. Solubilities were measured either by crystal weight-loss or by analysis of quench fluid by an isotope-dilution method. An experiment at 600 °C, 0.5 GPa in dilute 0.2 *m* NaCl yielded a solubility similar to that at 0.2 GPa at the same *T*. Ayers and Watson (1991) determined the solubility of natural monazite by weight loss at 1.0–2.8 GPa and 800–1100 °C, and also found no pressure dependence of solubility. However, Fig. 4 indicates that their solubility values are lower than would be predicted by extrapolation of a linear fit to the 0.2 GPa data of Gibert and Montel (1996) and Pourtier et al. (2010). Schmidt et al. (2007) measured solubility of monazite and xenotime at 800 °C and 2.0 GPa in a hydrothermal diamond-anvil cell by synchrotron-radiation X-ray fluorescence. Most experiments were done using acid solutions. However, one experiment on LaPO₄ in 4 *m*

NaCl ($X_{\text{NaCl}}=0.07$) at 800 °C and 1.1 GPa gave La concentrations at or below the detection limit of 0.6 millimolal. Assuming that LaPO₄ has a similar solubility in NaCl-bearing solutions as a function X_{NaCl} as CePO₄ (Eq. (1)), their measurement corresponds to a pure H₂O solubility of 0.15 millimolal (Fig. 4). This is similar to the CePO₄ solubility measured at the same *P* and *T* in the present study (0.045 ± 0.045 millimolal), but lower than our YPO₄ solubility (0.25 ± 0.04 millimolal). The very low solubilities obtained in this study in pure H₂O is supported by the trends with X_{NaCl} . Even if we had not measured CePO₄ or YPO₄ solubility in pure H₂O, extrapolation to pure H₂O from the NaCl-bearing experiments would give a solubility similar to what we measured. Taken together our results and those of Schmidt et al. (2007) imply substantially lower REE- or Y-phosphate solubility in pure H₂O than do the results of Ayers and Watson (1991), Gibert and Montel (1996) and Pourtier et al. (2010).

Possible reasons for the disparities in Fig. 4 include solubility contrasts between natural and synthetic minerals, intrinsic differences in the solubilities of the LREE and Y, differences in pressure, and discrepancies arising from varying experimental methods or starting materials. It is extremely unlikely that different solubilities of La, Ce, Nd and Y can account for the range of results given in Fig. 4. The very similar geochemical behavior of the REE and Y translate to only subtle solubility differences in a given fluid (e.g., Wood and Williams-Jones, 1994; Haas et al., 1995). This is supported by results of Schmidt et al. (2007) on a natural monazite, in which La and Nd were fractionated from Ce by 12% and 5%, respectively, in a 200 °C, 0.1 GPa, experimental fluid. In contrast, LaPO₄, CePO₄ and NdPO₄ solubilities in the high *PT* experimental studies differ by up to several orders of magnitude at any temperature. Similarly, a strong *P* dependence is not a plausible explanation as the required pressure dependence is negative, the opposite of that found for other oxide minerals (Dolejš and Manning, 2010). Moreover, where individual studies report solubilities at the same *T* and fluid composition but varying *P* (Ayers and Watson, 1991; Pourtier et al., 2010), any permissible *P* dependence is less than the uncertainties of the results.

Solubility results from synthetic orthophosphates involving a single cation should probably not be compared to those on natural monazite because of the presence of additional, soluble cations in the latter. At the same *P*, *T*, and fluid composition, we found that natural monazite was substantially more soluble than CePO₄. In addition, the large capsule geometry used by Ayers and Watson (1991) has been shown to promote growth of new crystals, which can be misinterpreted as quench. This problem evidently plagued their experiments on rutile and apatite (Tropper and Manning, 2005; Antignano and Manning, 2008a,b; Manning et al., 2008), though it is not clear that the same was true for monazite. Nevertheless, the combination of natural monazite and large-capsule geometry should conspire to produce apparent solubilities that are higher than those of synthetic monazites such LaPO₄, as CePO₄, or NdPO₄.

Because the capsule geometry and use of natural monazite in the Ayers and Watson (1991) study likely yielded apparent solubilities that were too high, their data should be treated as an upper bound. The maximum solubilities obtained in their study along with the results from Schmidt et al. (2007) and this work, are all lower than the measurements and/or extrapolated fit at 0.2 GPa from Gibert and Montel (1996) and Pourtier et al. (2010). This suggests an important difference between techniques or materials. Both of the latter studies used flux-grown NdPO₄, but Pourtier et al. (2010), using an isotope-dilution technique, showed that weight-loss and quench-fluid analysis gave similar results. Barring a combination of flux–melt inclusions and a systematic error in the isotope-dilution method, it is not clear why the results of these studies are so discrepant.

In summary, we find that CePO₄ and YPO₄ are only sparingly soluble in pure H₂O at high *P* and *T*. This is consistent with the results

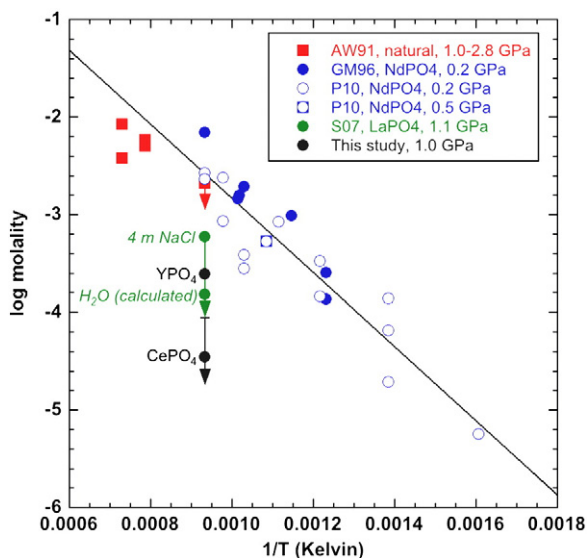


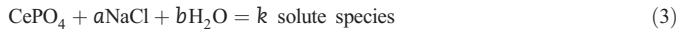
Fig. 4. Comparison of monazite solubility studies in initially pure H₂O or dilute H₂O–NaCl solutions (<4 *m* NaCl). Downward pointing arrows signify that plotted solubility is a maximum value. Results of Schmidt et al. (2007; S07) at 4 *m* NaCl were adjusted to pure H₂O by assuming the dependence on X_{NaCl} given in Eq. (1). This indicates good agreement between Schmidt et al. (2007) on LaPO₄ and the present work on CePO₄ and YPO₄. The data of Ayers and Watson (1991; AY91) on natural monazite are expected to give higher solubilities at a given *T* and *P* because of impurities such as Ca and Si are highly soluble in H₂O–NaCl (Newton and Manning, 2006). Assuming that their values are maxima, they also agree with Schmidt et al. (2007) and this study. In contrast the data of Gibert and Montel (1996; GM96) and Pourtier et al. (2010; P10) on NdPO₄ indicate a much higher solubility at a given *T*. The reasons for this discrepancy are unclear (see text).

of Schmidt et al. (2007) on LaPO₄. The use of natural monazite and possible material redistribution during experiments probably accounts for the greater solubilities of Ayers and Watson (1991) compared to this work and Schmidt et al. (2007). The solubilities returned by these studies as a group are lower at a given T than the solubility of NdPO₄ reported by Gibert and Montel (1996) and Poutier et al. (2010); however, the reason for the discrepancy is not clear and additional experiments are required to resolve this issue.

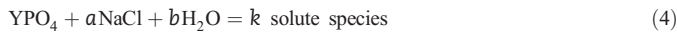
4.2. Solubility in H₂O–NaCl

The solubilities of CePO₄ and YPO₄ at 800 °C and 1 GPa increase with rising X_{NaCl}, but the dependence of relative solubility on salinity differs (Fig. 3). The increase in CePO₄ solubility with NaCl concentration is such that d²m_{CePO₄}/dX_{NaCl}² is positive, similar in form to apatite, fluorite, calcite and anhydrite, as reported by Antignano and Manning (2008a), Tropper and Manning (2007), Newton and Manning (2002) and Newton and Manning (2005), respectively. In contrast, YPO₄ solubility increases such that d²m_{YPO₄}/dX_{NaCl}² is negative, similar to the behavior of corundum, wollastonite and grossular (Newton and Manning, 2006, 2007). In pure H₂O and in solutions with low NaCl concentrations, YPO₄ is more soluble than CePO₄ in the range 0.00 < X_{NaCl} < 0.27 whereas above this value, CePO₄ is the more soluble phase.}}

To obtain information on the interaction of CePO₄ or YPO₄ with pure H₂O and NaCl + H₂O solutions, the following generalized dissolution reactions may be written (Newton and Manning, 2006, 2010):



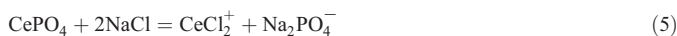
or



where *a* and *b* are the number of moles of NaCl and H₂O consumed to produce *k* moles of solutes per mole of orthophosphate dissolved. These reactions ignore molecular H₂O, which implicitly complete the inner-sphere solvation shells.

The relative molar proportions of H₂O and NaCl in Eqs. (3) and (4) were evaluated using the technique outlined in Newton and Manning (2006, 2010). Orthophosphate mole fractions were calculated assuming complete dissociation to Na⁺ and Cl[−] (Bradley, 1962; Aranovich and Newton, 1996; Newton and Manning, 2006). Fig. 5 shows the variation in the relative solubility enhancements, expressed as solute mole fraction at a given X_{NaCl} relative to that in pure H₂O (X°). The ratio X/X° thus represents the magnitude of solubility enhancement by a given NaCl mole fraction.

Values of logX/X° for CePO₄ rise with X_{NaCl} over the investigated range and are convex to salinity (Fig. 5). This implies that the activity of H₂O does not significantly influence CePO₄ solubility; i.e., *b* = 0 in Eq. (3). This and the positive dependence of solubility on the square of X_{NaCl} (Eq. (1)) in turn suggest that 2 moles of NaCl per mole of CePO₄ yield anhydrous solute species upon dissolution (*a* = 2). A simple (non-unique) equilibrium that could account for this relationship is



In contrast to CePO₄, the negative second derivative of YPO₄ molality with respect to X_{NaCl} points to a hydrous solute species. Fig. 5 shows that X/X° for YPO₄ increases to a maximum at X_{NaCl} ~ 0.33. Following Newton and Manning (2006), the NaCl mole fraction at which the maximum occurs, X_{NaCl}^{*}, defines the ratio of *a* to *b* in Eq. (4) via

$$X_{\text{NaCl}}^* = \frac{a}{a + b} \quad (6)$$

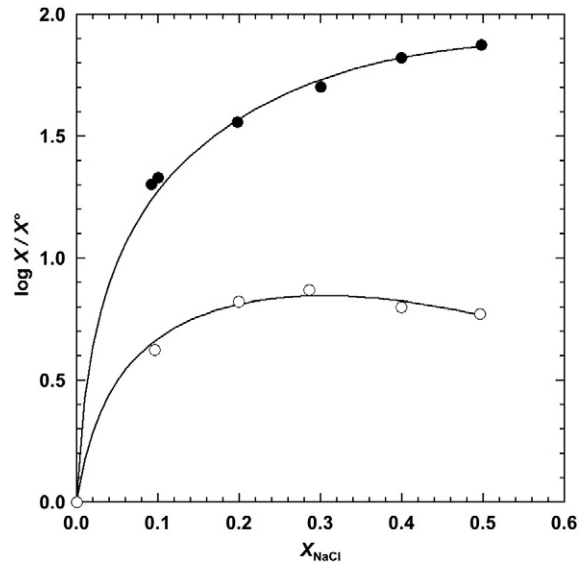
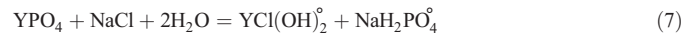


Fig. 5. Logarithm of the solubility enhancement, X/X°, versus X_{NaCl} at 800 °C and 1 GPa. Mole fractions of CePO₄ (filled circles) and YPO₄ (open circles) calculated assuming that NaCl is fully dissociated (see text). Solid lines calculated using Eqs. (1) and (2). The 2σ error bars are smaller than the symbol size. Continually rising X/X° for CePO₄ signifies anhydrous Ce–chloride complexing, whereas the maximum in X/X° for YPO₄ indicates Y complexing with both Cl and OH (see text).

The maximum at X_{NaCl}^{*} ~ 0.33 suggests that *a* = 1 and *b* = 2. A simple (non-unique) equilibrium that could account for this relationship is



The dissolution products proposed in Eqs. (5) and (7) suggest that, in NaCl-bearing fluids with neutral pH, the degree of Cl coordination for Y is lower than for Ce. Assuming similar geochemical behavior of Y and REE, this is consistent with the steric hindrance of chloride complexation with HREE relative to LREE proposed by Mayanovic et al. (2009).

Fig. 6 compares the X_{NaCl}-dependence of the solubility of CePO₄ and YPO₄ at 800 °C and 1 GPa with that of the Durango fluorapatite (Antignano and Manning, 2008a). The much greater increase in fluorapatite solubility with increasing NaCl concentration is consistent with its observed incongruent dissolution to REE phosphate + solutes (Antignano and Manning, 2008a). In addition, the different trends indicate that the solubility of the phosphate phases is controlled by Cl-cation complexation rather than Na-phosphate complexation. More generally, Fig. 6 highlights that ligand availability for REE/Y complexation will govern the dissolution and transport of these elements where apatite and/or orthophosphates are the main mineral hosts.

4.3. H₂O/Ce and subduction-zone fluids and melts

The H₂O/Ce ratio of subduction-zone magmas prior to crustal degassing has been proposed as a geothermometer for slab-fluid production (Plank et al., 2009). The similar partition coefficients of H₂O and Ce during mantle melting (Hauri et al., 2006) and their low background ratio in the mantle of ~200 (Dixon et al., 2002) make H₂O/Ce an optimal tracer for the addition of slab components to mantle-derived arc magmas. By considering Ce solubilities in fluids saturated in allanite or monazite, Plank et al. (2009) showed that H₂O/Ce should decrease in slab-top fluids by about four orders of magnitude from 600 to 1000 °C. Because H₂O/Ce in relatively undegassed melt inclusions from two study localities gave H₂O/Ce values corresponding to supersolidus temperatures, Plank et al. (2009) concluded that slab components are transported to the mantle source

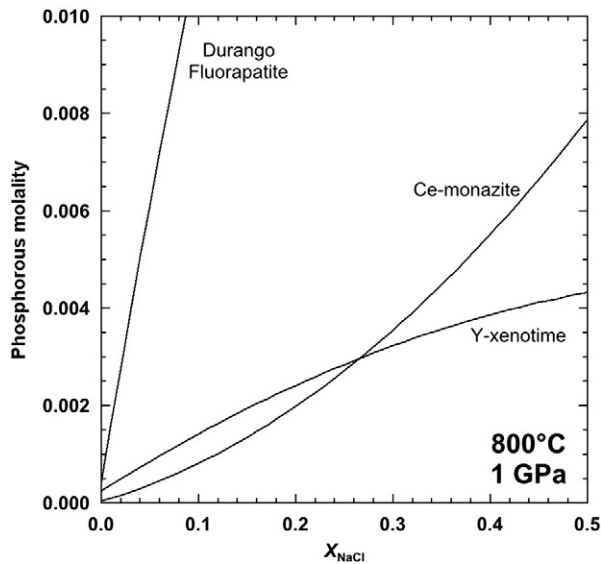


Fig. 6. Comparison between the solubility of fluorapatite (Antignano and Manning, 2008a) with that of CePO_4 and YPO_4 at 800 °C and 1 GPa. The much lower solubility of Ce-monazite and Y-xenotime at the same X_{NaCl} show that the control on phosphate mineral solubility is due to chloride complexing.

of arc magmas chiefly by either a slab melt or a silicate-rich hydrous fluid phase.

Fig. 7 shows $\text{H}_2\text{O}/\text{Ce}$ as a function of X_{NaCl} at 800 °C, 1 GPa, in a fluid saturated with Ce-monazite. Though the pressures of our experiments are lower than those expected for the slab–mantle interface at 800 °C (e.g., Syracuse et al., 2010), the effect of pressure is likely small compared to the effect of NaCl (Fig. 4). The very low solubility of CePO_4 in pure H_2O translates to an extremely high $\text{H}_2\text{O}/\text{Ce}$ of 2×10^5 (note that this is an upward revision of the monazite– H_2O datum in Fig. 1a from Plank et al., 2009). With increasing NaCl concentration, $\text{H}_2\text{O}/\text{Ce}$ declines dramatically, reaching 499 at $X_{\text{NaCl}} = 0.5$.

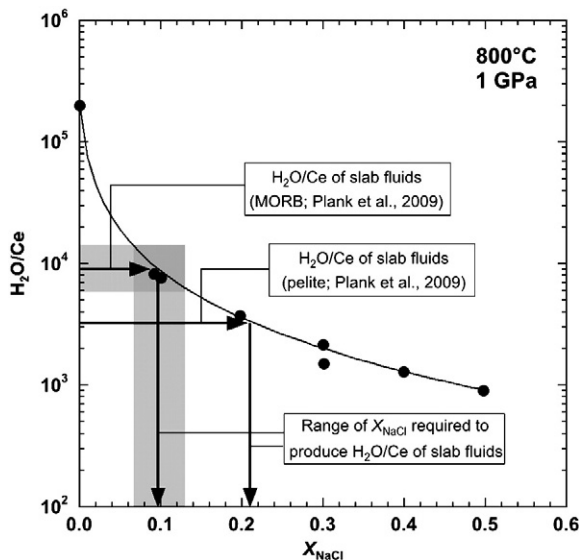


Fig. 7. $\text{H}_2\text{O}/\text{Ce}$ versus X_{NaCl} at 800 °C and 1 GPa, based on CePO_4 solubility data (filled circles) and Eq. (1) (solid line). The horizontal shaded rectangle represents the range of $\text{H}_2\text{O}/\text{Ce}$ inferred for 800 °C slab fluids (Plank et al., 2009). NaCl-bearing fluids produce this value at $X_{\text{NaCl}} = 0.10 \pm 0.03$. Cerium and H_2O transport by a NaCl brine could be an alternative to slab melts or silicate-rich H_2O , provided the NaCl concentration does not change significantly during transit to the site of arc-magma genesis.

Plank et al. (2009) inferred that at 800 °C, slab fluids have $\text{H}_2\text{O}/\text{Ce}$ of ~7000 to 15,000 (Fig. 7). Using Eq. (1), we find that in a H_2O –NaCl fluid at $X_{\text{NaCl}} = 0.10 \pm 0.03$ this range of ratios would result in a salinity that is not uncommon for a wide range of metamorphic settings (e.g., Yardley and Graham, 2002). Thus, NaCl-bearing fluids of moderate salinity offer another mechanism by which to produce the $\text{H}_2\text{O}/\text{Ce}$ ratio characteristic of arc-magma source regions. However, a caveat is that this mechanism requires little shift in the NaCl concentration from liberation at the slab to the site of melting.

4.4. Cl-bearing fluids and the implications for REE transport in the deep crust

Field studies in high-grade rocks show that mobility of REE and Y is greatly enhanced in the presence of brines (e.g. Newton et al., 1998; Harlov et al., 2006; Hetherington and Harlov, 2008; Hansen and Harlov, 2009; Glassley et al., 2010). Most experimental attempts to explain REE or Y mobility in this or other settings have focused on chloride complexing at acidic pH, where solubilities of these elements are indeed elevated relative to values at acid–base neutrality. However, in metamorphic environments of low to modest water–rock ratios, the high solubilities of the major rock-forming elements provides the capacity to buffer pH at the near-neutral to alkaline pH values of feldspar–mica–quartz or amphibole–pyroxene–plagioclase–quartz assemblages, suggesting that the acidic pH that is implicitly or explicitly invoked to explain REE and Y mobility is unlikely. Our results offer a simple alternative to REE and Y transport by acid–chloride solutions. The strong enhancement of CePO_4 and YPO_4 solubilities by NaCl points to major REE and Y mobility at neutral pH, even at only modest salinity. Where concentrated NaCl brines occur, REE and Y mobility may be profound.

5. Conclusions

1. Ce-monazite and Y-xenotime are sparingly soluble in pure H_2O at 800 °C and 1 GPa. Our measured values of 0.045 ± 0.045 and 0.25 ± 0.04 millimolar for CePO_4 and YPO_4 , respectively, are similar to the value reported by Schmidt et al. (2007) for LaPO_4 . Natural monazite gives higher solubility. This and possible material redistribution during experiments may explain the high solubilities obtained by Ayers and Watson (1991). However, together this group of measurements is in conflict with the data set of Gibert and Montel (1996) and Pourtier et al. (2010) at 0.2 GPa over a range of temperatures. The reason for the disagreement is not known, and additional experiments are needed to resolve the discrepancy.
2. The solubilities of CePO_4 and YPO_4 are progressively enhanced by the addition of NaCl to H_2O ; however, the form of the dependence on X_{NaCl} differs between the two phases. With addition of NaCl, CePO_4 solubility rises to an increasing degree, whereas YPO_4 rises to a decreasing degree. Solubilities of CePO_4 and YPO_4 at $X_{\text{NaCl}} = 0.5$ are greater than in pure H_2O by factors of 223 and 18, respectively.
3. YPO_4 is at least 1.5 times more soluble than CePO_4 in pure H_2O at 800 °C and 1 GPa, and its solubility remains greater than that of CePO_4 at $X_{\text{NaCl}} = 0.27$. Although this appears to contradict the more common occurrence of monazite than xenotime metasomatic settings, it probably simply highlights the fact that REE and Y solubilities are a complex function of the concentrations of a range of ligands in natural fluids.
4. Stoichiometric analysis of the solubility enhancements reveals that the dominant solute species of Ce are anhydrous Ce-chlorides, whereas Y dissolves as mixed Cl–OH species. The decrease in the degree of chloride complexation is consistent with independent studies of REE complexation in acidic chloride solutions (Mayanovic et al., 2009). Phosphate complexes with $\text{Na} \pm \text{H}$.
5. The results have important implications for REE and Y transport by geologic fluids. For example, the $\text{H}_2\text{O}/\text{Ce}$ ratio is an important tracer of slab fluids in subductions zones. The data show that CePO_4

dissolution into an H₂O–NaCl fluid with $X_{\text{NaCl}} \sim 0.1$ can produce H₂O/Ce identical to that inferred for slab fluids at 800 °C. This provides an alternative to transport of slab components by melts or silicate-rich fluids. More generally, the enhancement in solubility by neutral NaCl-bearing H₂O provides an alternative to acidic chloride solutions for promoting REE mobility in the middle to deep crust where extremes of pH are unlikely.

Acknowledgments

The authors wish to thank R.C. Newton for his generous help with the experiments and the discussions. This study was supported by NSF grant EAR 0711521 to CEM. S. Klemme is thanked for his helpful review and D. Dingwell for the editorial handling of the manuscript.

References

- Andrehs, G., Heinrich, W., 1998. Experimental determination of REE distributions between monazite and xenotime: potential for temperature-calibrated geochronology. *Chemical Geology* 149, 83–96.
- Antignano, A., Manning, C.E., 2008a. Fluorapatite solubility in H₂O and H₂O–NaCl at 700 to 900 °C and at 0.7 to 2.0 GPa. *Chemical Geology* 251, 112–119.
- Antignano, A., Manning, C.E., 2008b. Rutile solubility in H₂O, H₂O–SiO₂, and H₂O–NaAlSi₃O₈ fluids at 0.7–2.0 GPa and 700–1000 °C: implications for mobility of nominally insoluble elements. *Chemical Geology* 255, 283–293.
- Aranovich, L.Y., Newton, R.C., 1996. H₂O activity in concentrated NaCl solutions at high pressures and temperatures measured by the brucite–periclae equilibrium. *Contributions to Mineralogy and Petrology* 125, 200–212.
- Ayers, J.C., Watson, E.B., 1991. Solubility of apatite, monazite, zircon and rutile in supercritical aqueous fluids with implications for subduction zone geochemistry. *Philosophical Transactions of the Royal Society A* 335, 365–375.
- Bingen, B., Demaiffe, D., Hertogen, J., 1996. Redistribution of rare earth elements, thorium and uranium over accessory minerals in the course of amphibolite to granulite-facies metamorphism: the role of apatite and monazite in orthogneisses from southwestern Norway. *Geochimica et Cosmochimica Acta* 60, 1341–1354.
- Boatner, L.A., 2002. Synthesis, structure, and properties of monazite, pretulite, and xenotime. *Reviews in Mineralogy and Geochemistry* 48, 87–121.
- Boatner, L.A., Sales, B.C., 1988. Monazite. In: Lutze, W., Ewing, R.C. (Eds.), *Radioactive Waste Forms for the Future*. Elsevier, Amsterdam, pp. 495–564.
- Bohlen, S.R., 1984. Equilibria for precise pressure calibration and a frictionless furnace assembly for the piston-cylinder apparatus. *Neues Jahrbuch für Mineralogie Monatshefte* 9, 404–412.
- Bosse, V., Boulvais, P., Gautier, P., Tiepolo, M., Ruffet, G., Devidal, J.L., Cherneva, Z., Gerdjikov, I., Paquette, J.L., 2009. Fluid-induced disturbance of the monazite Th–Pb chronometer: in situ dating and element mapping in pegmatites from the Rhodope (Greece, Bulgaria). *Chemical Geology* 261, 286–302.
- Bradley, R.S., 1962. Thermodynamic calculations on phase equilibria involving fused salts. Part I. General theory and application to equilibria involving calcium carbonate at high pressure. *American Journal of Science* 260, 374–382.
- Caciagli, N.C., Manning, C.E., 2003. The solubility of calcite in water at 5–16 kbar and 500–800 °C. *Contributions to Mineralogy and Petrology* 146, 275–285.
- Cesbron, F., 1989. Mineralogy of the rare-earth elements. In: Möller, P., Cerny, P., Saupe, F. (Eds.), *Lanthanides, Tantalum and Niobium*. Mineralogy, Geochemistry, Characteristics of Primary Ore Deposits, Prospecting, Processing, and Applications. Springer-Verlag, pp. 3–26.
- Cetiner, Z.S., Wood, S.A., Gammons, C.H., 2005. The aqueous geochemistry of the rare earth elements. Part XIV. The solubility of rare earth element phosphates from 23 to 150 °C. *Chemical Geology* 214, 147–169.
- Cherniak, D.J., Pyle, J., Rakovan, J., 2004. Synthesis of REE and Y phosphates by Pb-free flux methods and their utilization as standards for electron microprobe analysis and in design of monazite chemical U–Th–Pb dating protocol. *American Mineralogist* 89, 1533–1539.
- Corrie, S.L., Kohn, M.J., 2008. Trace-element distributions in silicates during prograde metamorphic reactions: implications for monazite formation. *Journal of Metamorphic Geology* 26, 451–464.
- Cuney, M., Friedrich, M., 1987. Physicochemical and crystal-chemical controls on accessory mineral paragenesis in granulites: implications for uranium metallogenesis. *Bulletin de Minéralogie* 110, 235–247.
- Devidal, J.L., Gibert, F., Kieffer, B., Pin, C., Montel, J.M., 1998. A new method for solubility measurement: application to NdPO₄ system in H₂O–NaCl–HCl hydrothermal fluids. *Mineralogical Magazine* 62, 375–376.
- Dixon, J.E., Leist, L., Langmuir, C., Schilling, J.G., 2002. Recycled dehydrated lithosphere observed in plume-influenced mid-ocean-ridge basalt. *Nature* 420, 385–389.
- Dolejš, D., Manning, C.E., 2010. Thermodynamic model for mineral solubility in aqueous fluids: theory, calibration, and application to model fluid-flow systems. *Geofluids* 10, 20–40.
- Ewing, R.C., 2001. The design and evaluation of nuclear-wasteforms: clues from mineralogy. *Canadian Mineralogist* 39, 697–715.
- Ewing, R.C., Wang, L., 2002. Phosphates as nuclear waste forms. *Reviews in Mineralogy and Geochemistry* 48, 673–699.
- Gibert, F., Montel, J.M., 1996. Étude expérimentale de la solubilité de la monazite dans des fluides à H₂O–CO₂. *Réunion des Sciences de la Terre* 16.
- Gieré, R., 1996. Formation of rare earth minerals in hydrothermal systems. In: Jones, A. P., Wall, F., Williams, C.T. (Eds.), *Rare Earth Minerals*. Chapman and Hall, pp. 105–150.
- Glassley, W.E., Korstgard, J.A., Sorensen, K., 2010. K-rich brine and chemical modification of the crust during continent–continent collision, Nagssugtoqidian Orogen, West Greenland. *Precambrian Geology* 180, 47–62.
- Gratz, R., Heinrich, W., 1997. Monazite–xenotime thermobarometry: experimental calibration of the miscibility gap in the binary system CePO₄–YPO₄. *American Mineralogist* 82, 772–780.
- Haas, J.R., Shock, E.L., Sassani, D.C., 1995. Rare earth elements in hydrothermal systems: estimates of standard partial molal thermodynamic properties of aqueous complexes of the rare earth elements at high pressures and temperatures. *Geochimica et Cosmochimica Acta* 59, 4329–4350.
- Hansen, E.C., Harlov, D.E., 2009. Orthophosphate and biotite chemistry from orthopyroxene-bearing migmatites from California and South India: the role of a fluid-phase in the evolution of granulite-facies migmatites. *Mineralogy and Petrology* 95, 201–217.
- Harlov, D.E., Johansson, L., Van den Kerkhof, A., Förster, H.-J., 2006. The role of advective fluid flow and diffusion during localized, solid-state dehydration: Söndrum Stenuggeriet, Halmstad, SW Sweden. *Journal of Petrology* 47, 3–33.
- Harrison, T.M., Catlos, E.J., Montel, J.M., 2002. U–Th–Pb dating of phosphate minerals. *Reviews in Mineralogy and Geochemistry* 48, 523–577.
- Hauri, E.H., Gaetani, G.A., Green, T.H., 2006. Partitioning of water during melting of the Earth's upper mantle at H₂O-undersaturated conditions. *Earth and Planetary Science Letters* 248, 715–734.
- Hetherington, C.J., Harlov, D.E., 2008. Metasomatic thorite and uraninite inclusions in xenotime and monazite from granitic pegmatites, Hidra anorthosite massif, southwestern Norway: mechanics and fluid chemistry. *American Mineralogist* 93, 806–820.
- Janots, E., Engi, M., Berger, A., Allaz, J., Schwarz, J.O., Spandler, C., 2008. Prograde metamorphic sequence of REE-minerals in pelitic rocks of the Central Alps: implications on allanite–monazite–xenotime phase relations from 250 to 610 °C. *Journal of Metamorphic Geology* 26, 509–526.
- Janots, E., Engi, M., Rubatto, D., Berger, A., Gregory, C., Rahn, M., 2009. Metamorphic rates in collisional orogeny from in situ allanite and monazite dating. *Geology* 37, 11–14.
- Keppler, H., 1996. Constraints from partitioning experiments on the composition of subduction-zone fluids. *Nature* 380, 237–240.
- Kohn, M.J., Malloy, M.A., 2004. Formation of monazite via prograde metamorphic reactions among common silicates: implications for age determinations. *Geochimica et Cosmochimica Acta* 68, 101–113.
- Manning, C.E., Boettcher, S.L., 1994. Rapid-quench hydrothermal experiments at mantle pressures and temperatures. *American Mineralogist* 79, 1153–1158.
- Manning, C.E., Wilke, M., Schmidt, C., Cauzid, J., 2008. Rutile solubility in albite–H₂O and Na₂Si₂O₇–H₂O at high temperatures and pressures by in-situ synchrotron radiation micro-XRF. *Earth and Planetary Science Letters* 272, 730–737.
- Markl, G., Bucher, K., 1998. Composition of fluids in the lower crust inferred from metamorphic salt in lower crustal rocks. *Nature* 391, 781–783.
- Markl, G., Ferry, J.M., Bucher, K., 1998. Formation of saline brines and salt in the lower crust by hydration reactions in partially retrogressed granulites from the Lofoten Islands, Norway. *American Journal of Science* 298, 705–757.
- Mayanovic, R.A., Anderson, A.J., Basset, W.A., Chou, I.M., 2009. Steric hindrance and the enhanced stability of light rare-earth elements in hydrothermal fluids. *American Mineralogist* 94, 1487–1490.
- Miller, C.F., Mittlefehldt, D.W., 1982. Depletion of rare-earth elements in felsic magmas. *Geology* 10, 129–133.
- Montel, J.M., 1986. Experimental determination of the solubility of Ce–monazite in SiO₂–Al₂O₃–K₂O–Na₂O melts at 800 °C, 2 kbar, under H₂O-saturated conditions. *Geology* 14, 659–662.
- Montel, J.M., 1993. A model for monazite/melt equilibrium and application to the generation of granitic magmas. *Chemical Geology* 110, 127–146.
- Nadeau, S., Philippot, P., Pineau, F., 1993. Fluid inclusion and mineral isotopic compositions (H–C–O) in eclogitic rocks as tracers of local fluid migration during high-pressure metamorphism. *Earth and Planetary Science Letters* 114, 431–448.
- Newton, R.C., Manning, C.E., 2002. Experimental determination of calcite solubility in H₂O–NaCl solutions at deep crust/upper mantle pressures and temperatures: implications for metasomatic processes in shear zones. *American Mineralogist* 87, 1401–1409.
- Newton, R.C., Manning, C.E., 2005. Solubility of anhydrite, CaSO₄, in NaCl–H₂O solutions at high pressures and temperatures: applications to fluid–rock interaction. *Journal of Petrology* 46, 701–716.
- Newton, R.C., Manning, C.E., 2006. Solubilities of corundum, wollastonite and quartz in H₂O–NaCl solutions at 800 °C and 10 kbar: interaction of simple minerals with brines at high pressure and temperature. *Geochimica et Cosmochimica Acta* 70, 5571–5582.
- Newton, R.C., Manning, C.E., 2007. Solubility of grossular, Ca₃Al₂Si₃O₁₂, in H₂O–NaCl solutions at 800 °C and 10 kbar, and the stability of garnet in the system CaSiO₃–Al₂O₃–H₂O–NaCl. *Geochimica et Cosmochimica Acta* 71, 5191–5202.
- Newton, R.C., Manning, C.E., 2010. Role of saline fluids in deep-crustal and upper-mantle metasomatism: insights from experimental studies. *Geofluids* 10, 58–72.
- Newton, R.C., Aranovich, L.Y., Hansen, E.C., Vandenheue, B.A., 1998. Hypersaline fluids in Precambrian deep-crustal metamorphism. *Precambrian Research* 91, 41–63.
- Overstreet, W.C., 1967. The Geological Occurrence of Monazite. U.S. Geological Survey Professional Paper 530. 327 pp.

- Pan, Y.M., Fleet, M.E., 2002. Compositions of the apatite-group minerals: substitution mechanisms and controlling factors. *Reviews in Mineralogy and Geochemistry* 48, 13–49.
- Philippot, P., Selverstone, J., 1991. Trace element-rich brines in eclogitic veins: implications for fluid compositions and transport during subduction. *Contributions to Mineralogy and Petrology* 106, 417–430.
- Plank, T., Cooper, L., Manning, C.E., 2009. Emerging geothermometers for estimating slab surface temperatures. *Nature Geoscience* 2, 611–615.
- Poitrasson, F., Chenery, S., Bland, D.J., 1996. Contrasted monazite hydrothermal alteration mechanisms and their geochemical implications. *Earth and Planetary Science Letters* 145, 79–96.
- Poitrasson, F., Chenery, S., Shepherd, T.J., 2000. Electron microprobe and LA-ICP-MS study of monazite hydrothermal alteration: implications for U–Th–Pb geochronology and nuclear ceramics. *Geochimica et Cosmochimica Acta* 64, 3283–3297.
- Poitrasson, F., Oelkers, E., Schott, J., Montel, J.M., 2004. Experimental determination of synthetic NdPO_4 monazite solubility in water from 21 °C to 300 °C: implications for rare earth element mobility in crustal fluids. *Geochimica et Cosmochimica Acta* 68, 2207–2221.
- Pourtier, E., Devidal, J.L., Gibert, F., 2010. Solubility measurements of synthetic neodymium monazite as a function of temperature at 2 kbars, and aqueous neodymium speciation in equilibrium with monazite. *Geochimica et Cosmochimica Acta* 74, 1872–1891.
- Pyle, J.M., Spear, F.S., 1999. Yttrium zoning in garnet: coupling of major and accessory phases during metamorphic reactions. *Geological Materials Research* 1, 1–49.
- Pyle, J.M., Spear, F.S., 2000. An empirical garnet (YAG)-xenotime thermometer. *Contributions to Mineralogy and Petrology* 138, 51–58.
- Pyle, J.M., Spear, F.S., Rudnick, R.L., McDonough, W.F., 2001. Monazite–xenotime–garnet equilibrium in metapelites and a new monazite–garnet thermometer. *Journal of Petrology* 42, 2083–2107.
- Rapp, R.P., Watson, E.B., 1986. Monazite solubility and dissolution kinetics – implications for the thorium and light rare-earth chemistry of felsic magmas. *Contributions to Mineralogy and Petrology* 94, 304–316.
- Rapp, J.F., Klemme, S., Butler, I.B., Harley, S.L., 2010. Extremely high solubility of rutile in chloride and fluoride-bearing metamorphic fluids: an experimental investigation. *Geology* 38, 323–326.
- Read, D., Williams, C.T., 2001. Degradation of phosphatic wasteforms incorporating long-lived radioactive isotopes. *Mineralogical Magazine* 65, 589–601.
- Roland, Y., Cox, S., Boullier, A.M., Pennacchioni, G., Mancktelow, N., 2003. Rare earth and trace element mobility in mid-crustal shear zones: insights from the Mont Blanc Massif (Western Alps). *Earth and Planetary Science Letters* 214, 203–219.
- Scambelluri, M., Philippot, P., 2001. Deep fluids in subduction zones. *Lithos* 55, 213–227.
- Scambelluri, M., Philippot, P., Pennacchioni, G., 1998. Salt-rich aqueous fluids formed during eclogitization of metabasites in the Alpine continental crust (Austroalpine Mt. Emilius unit, Italian western Alps). *Lithos* 43, 151–161.
- Schmidt, C., Rickers, K., Bilderback, D.H., Huang, R., 2007. In situ synchrotron radiation XRF study of REE phosphate dissolution in aqueous fluids to 800 °C. *Lithos* 95, 87–102.
- Selverstone, J., Franz, G., Thomas, S., Getty, S., 1992. Fluid variability in 2 GPa eclogites as an indicator of fluid behavior during subduction. *Contributions to Mineralogy and Petrology* 112, 314–357.
- Seydoux-Guillaume, A.-M., Paquette, J.-L., Wiedenbeck, M., Montel, J.-M., Heinrich, W., 2002. Experimental resetting of the U–Th–Pb systems in monazite. *Chemical Geology* 191, 165–181.
- Spear, F.S., Pyle, J.M., 2002. Apatite, monazite and xenotime in metamorphic rocks. *Reviews in Mineralogy and Geochemistry* 48, 293–335.
- Syracuse, E.M., van Keken, P.E., Abers, G.A., 2010. The global range of subduction zone thermal models. *Physics of the Earth and Planetary Interiors* 183, 73–90.
- Touret, J.L.R., 1985. Fluid regime in Southern Norway: the record of fluid inclusions. In: Tobi, A.C., Touret, J.L.R. (Eds.), *The Deep Proterozoic Crust in the North Atlantic Provinces*. Reidel, Dordrecht, pp. 517–549.
- Touret, J.L.R., 2001. Fluids in metamorphic rocks. *Lithos* 55, 1–25.
- Townsend, K.J., Miller, C.F., D'Andrea, J.L., Ayers, J.C., Harrison, T.M., Coath, C.D., 2000. Low-temperature replacement of monazite in the Ireteba granite, southern Nevada: geochronological implications. *Chemical Geology* 172, 95–112.
- Tropper, P., Manning, C.E., 2005. Very low solubility of rutile in H_2O at high pressure and temperature, and its implications for Ti-mobility in subduction zones. *American Mineralogist* 90, 502–505.
- Tropper, P., Manning, C.E., 2007. The solubility of fluorite in H_2O and H_2O – NaCl at high pressure and temperature. *Chemical Geology* 242, 299–306.
- Wing, B.A., Ferry, J.M., Harrison, T.M., 2003. Prograde destruction and formation of monazite and allanite during contact and regional metamorphism of pelites: petrology and geochronology. *Contributions to Mineralogy and Petrology* 145, 228–250.
- Wood, S.A., 1990a. The aqueous geochemistry of the rare-earth elements and yttrium. 1. Review of available low-temperature data for inorganic complexes and the inorganic REE speciation of natural waters. *Chemical Geology* 82, 159–186.
- Wood, S.A., 1990b. The aqueous geochemistry of the rare-earth elements and yttrium. 1. Theoretical predictions of speciation in hydrothermal solutions to 350 °C at saturation water vapor pressure. *Chemical Geology* 88, 99–125.
- Wood, S.A., Williams-Jones, A.E., 1994. The aqueous geochemistry of the rare-earth elements and yttrium: 4. Monazite solubility and REE mobility in exhalative massive sulfide-depositing environments. *Chemical Geology* 115, 47–60.
- Yardley, B.W.D., Graham, J.T., 2002. The origins of salinity in metamorphic fluids. *Geofluids* 2, 249–256.